The Canadian Mineralogist
Vol. 33, pp. 279-292 (1995)

THEORY, PRACTICE AND APPLICATION OF MICRO-PIXE ANALYSIS AND ELEMENT-DISTRIBUTION MAPS

JOHN L. CAMPBELL AND WILLIAM J. TEESDALE

Department of Physics, University of Guelph, Guelph, Ontario N1G 2W1

NORMAN M. HALDEN

Department of Geological Sciences, University of Manitoba, Winnipeg, Manitoba R3T 2N2

ABSTRACT

Micro-PIXE (*P*roton *I*nduced *X*-ray *E*mission) analysis is the proton analogue of electron-probe micro-analysis. A 2–4 MeV beam of protons, produced using an electrostatic accelerator, is focused to a micrometer spot-size on a specimen, and the emitted X-ray flux is analyzed using a Si(Li) detector. The high magnetic rigidity of the beam requires magnetic or electrostatic quadrupole lenses in contrast to the cylindrically symmetrical electrostatic lenses used with electron beams. Several factors constrain the geometry of an end-station: (i) to minimize thermal effects resulting from the high densities of current required for low limits of detection, it is necessary to have the detector close to the sample; (ii) a high-magnification microscope using transmitted and reflected light is necessary to be able to direct the beam onto samples mounted on a motorized X–Y–Z stage; (iii) multi-element analysis necessitates the use of X-ray absorbing filters between the sample and detector. X-ray data are recorded in a multichannel analyzer and processed using a dedicated PIXE data-processing program. On-demand beam-deflection reduces pulse pile-up in X-ray spectra. Samples are analyzed using a dual analysis protocol; concentrations of major and minor elements are determined first, followed by those of trace elements. Analysis of homogeneous standards indicates that matrix effects are understood. Detection limits for geologically important trace elements such as Cr, Ni, Sr, Rb, Y, Nb, Zr, U and Pb are usually in the 1 – 20 ppm range. In the scanning proton microprobe (SPM), distribution maps of elements are recorded by rastering a proton beam across a sample using electrostatic or magnetic fields. Most SPM systems permit the on-line display of a number of 1-*D* or 2-*D* element images on a graphics workstation.

Keywords: micro-PIXE, proton microprobe, *in situ* trace-element analysis, line scans, 2-D imaging.

SOMMAIRE

L'analyse chimique par émission de rayons X induite par faisceau protonique (micro-PIXE) est l'analogue protonique de l'analyse par microsonde électronique. Un faisceau de protons d'une puissance de 2–4 MeV, issu d'un accélérateur électrostatique, est focalisé sur un point de dimensions micrométriques sur un échantillon, et le flux de rayons X émis est analysé au moyen d'un détecteur Si(Li). La grande rigidité magnétique du faisceau requiert des lentilles magnétiques et électrostatiques quadrupolaires, au lieu des lentilles cylindriquement symétriques servant à focaliser un faisceau d'électrons. Plusieurs facteurs exercent des contraintes géométriques sur la conception d'un poste d'observation: (i) afin de minimiser les effets thermiques des densités élevées de courant requises pour atteindre un faible seuil de détection, il s'avère nécessaire de placer le détecteur tout près de l'échantillon; (ii) un microscope optique à fort grossissement, utilisé avec lumière transmise et réfléchie, est nécessaire afin de diriger le faisceau sur les échantillons, positionnés sur une platine X–Y–Z munie de moteurs; (iii) une analyse chimique d'un échantillon pour plusieurs éléments requiert l'insertion de filtres visant à absorber des rayons X, placés entre échantillon et détecteur. Les données de rayons X sont enregistrées par un analyseur à multicanaux, et manipulées avec un logiciel consacré à cette opération. Une déviation du faisceau sur demande réduit l'empilement des spectes de rayons X émis. Les échantillons sont analysés selon un protocole d'analyse double; on détermine d'abord la concentration des éléments majeurs et mineurs, et ensuite celle des éléments traces. L'analyse d'étalons homogènes assure la compréhension des effets dus à la matrice. Les seuils de détection des éléments traces jugés importants dans les applications géologiques, comme Cr, Ni, Sr, Rb, Y, Nb, Zr, U et Pb, sont normalement de l'ordre de 1 à 20 ppm. Dans le cas de la microsonde protonique à balayage, les cartes de distribution des éléments sont enregistrées en balayant le faisceau sur la surface d'un échantillon au moyen de champs électrostatiques et magnétiques. La plupart des systèmes à balayage permettent la visualisation graphique directe de bon nombre d'images de distribution dans une ou deux dimensions sur écran.

(Traduit par la Rédaction)

Mots-clés: méthode micro-PIXE, microsonde protonique, analyse *in situ*, éléments traces, profils linéaires, distribution dans deux dimensions.

INTRODUCTION

The proton microprobe (Watt & Grime 1987) is the proton analogue of the electron microprobe; it delivers a focused beam of charged particles to a specimen, which emits X rays characteristic of its elemental constituents and their concentrations. The X-ray spectrum is recorded in energy-dispersion mode by a Si(Li) detector. Proton-induced X-ray emission with such a microbeam (micro-PIXE) provides spatial resolution similar to that of the electron microprobe (~1 μm), but offers significantly lower limits of detection, commonly in the 1 – 20 ppm range. Individual mineral grains may be analyzed *in situ*, or the beam may be rastered to provide 1- or 2-dimensional images of element distribution. The beam currents required for analysis at an economic rate do not usually cause significant damage to the specimen.

PIXE is now a well-established technique (Johansson & Campbell 1988), and fully quantitative procedures have been developed to provide accurate determination of concentrations of major, minor and trace elements. These procedures have much in common with electron probe micro-analysis (EPMA). However, the underlying physics is much simpler than in the case of electron-beam excitation, and matrix effects can be dealt with in a straightforward manner, a significant advantage from the viewpoint of quantitative analysis. Standardization procedures are simple and direct. Demonstration publications (*e.g.*, Campbell *et al.* 1990, Ryan *et al.* 1990), focusing on the potential of micro-PIXE in geochemistry and mineralogy, are now being superseded by papers reporting use of the mature technique in well-defined problems in the Earth Sciences. Reviews have been presented by MacArthur & Ma (1991), Sie *et al.* (1991) and Ryan & Griffin (1993). An attractive aspect of the proton (or nuclear) microprobe is that PIXE can be supplemented by other techniques of ion-beam analysis such as Rutherford back-scattering and proton-induced gamma-ray emission.

This paper outlines the micro-PIXE technique and examines the issue of quantitative analysis of mineralogical and geological specimens. The following paper (Halden *et al.* 1995a) surveys a variety of applications of the technique. The characteristic X-ray yield from any element increases with increasing energy of the protons, E_p, but most small accelerators are limited to about 3 MeV, and higher beam-energies prove not of significant advantage, as the spectral background due to gamma-ray production increases. At a given E_p, the X-ray yield from a particular element decreases rapidly with atomic number, *Z*. Finally, the *bremsstrahlung* background in PIXE is a secondary phenomenon, arising in the main from the secondary electrons ejected by protons, as opposed to the protons themselves; peak-to-background ratios are therefore commonly much greater in PIXE than in EPMA. As a result, PIXE in many cases provides detection limits of a few ppm in a spot analysis, and can be used for trace-element mapping.

EXPERIMENTAL

Beam production

The proton beam is supplied typically by a small electrostatic accelerator. The maturing of PIXE and other techniques of ion-beam analysis has helped drive technological improvements in small accelerators in the last few years. Figure 1 shows the similarity of the proton microprobe to the electron microprobe, and also to the synchrotron X-ray fluorescence microprobe. Whereas in the electron probe, electrostatic lenses of cylindrical symmetry provide the focusing, such lenses cannot cope with the much higher magnetic rigidity of 2 – 4 MeV protons, which require the rather bulkier electric- or magnetic-quadrupole lenses. The beam is directed onto a small aperture that acts as the object for the system of demagnifying lenses, usually a doublet, triplet or quadruplet of magnetic quadrupoles. The parasitic aberrations of these lenses must be minimized if micrometric beam-spots are to be obtained. One line of lens development has culminated in wide-bore lenses formed by high-precision machining from a single piece of iron (*e.g.*, Grime *et al.* 1991). Another approach (Martin & Goloskie 1988) uses narrow-bore lenses, which require much less power and hence no cooling: in this case, auxiliary magnetic-dipole and electric-quadrupole fields are used to cancel the non-quadrupole components and to compensate for rotational aberration; such a system is used at Guelph. The chamber pressure must be below 10^{-4} Pa to avoid defocusing of the beam due to scattering by residual gas. Beams of several nA current in a 10 × 10 μm spot are routine, and several laboratories (Grime *et al.* 1991, Legge *et al.* 1993) have reported spots of less than 1 μm across with sufficient current to conduct a PIXE analysis.

Owing to X-ray attenuation, the depth probed in a specimen is somewhat less than the full depth of penetration of the beam; Table 1 shows some representative

TABLE 1. REPRESENTATIVE VALUES OF D_{90} FOR 3 MeV PROTONS

	Pentlandite	Chromite	Quartz	Zircon
Ni	14.1 (μm)	12.3 (μm)	38.9 (μm)	21.2 (μm)
Se	18.8	19.0	40.6	26.5
Mo	24.9	21.1	39.9	27.6
Pd	25.9	21.3	39.4	24.9
Sn	26.2	21.2	38.9	25.7
W	12.1	15.2	40.6	23.7
Pb	18.5	18.5	41.3	26.5
U	22.7	20.7	41.1	27.8

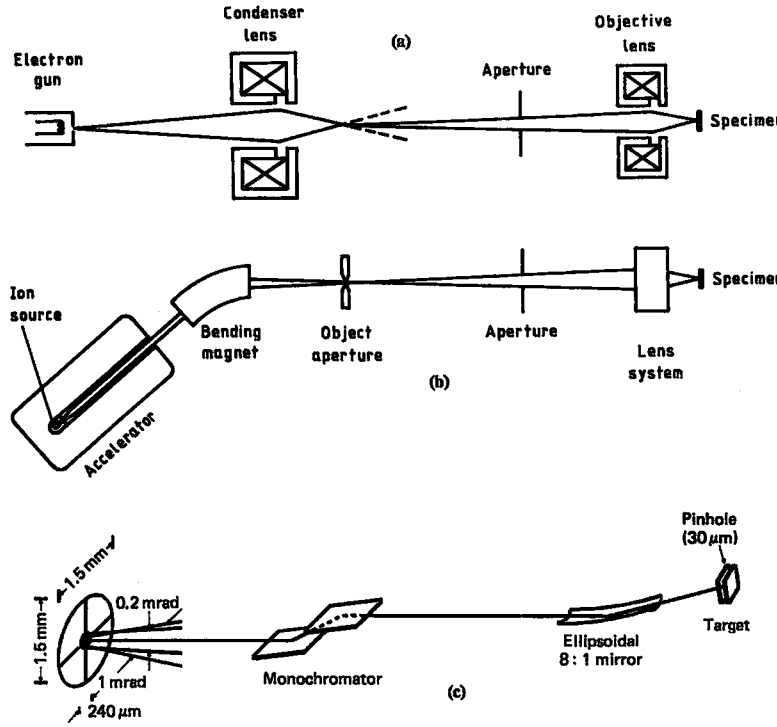

FIG. 1. Schematic of (a) electron, (b) proton and (c) synchrotron X-ray microprobes.

values of D_{90}, the depth above which 90% of observed X-rays originate. Note that D_{90} varies for the different elements in a given mineral, and that it is significantly larger than the typical 1 μm values of EPMA. In most cases, spot analysis of minerals is done with a beam that is 5 – 30 μm wide. These dimensions are similar to D_{90}, and they provide a degree of averaging over the area of the specimen. Except in the study of fine chemical zoning, there is no particular merit in using a highly focused beam. Use of 5 – 30 μm beams in spot analysis reduces specimen heating load and diminishes the possibility of specimen damage. For cases of chemical zoning, it follows that a beam of width significantly less than the zone width is required, in order to guarantee that only the particular zone of interest is sampled by the beam.

Specimen chamber

The chamber resembles that of the electron probe, its principal components being a motor-driven stage, a high-magnification microscope for optical viewing of the specimen, and a Si(Li) X-ray detector. A large-area detector placed as near the specimen as possible helps minimize the beam current needed. Specimens have to be polished and carbon-coated, and either "thick" specimens or thin sections may be used. In the latter case, thicknesses of at least 50 μm are required to prevent protons from penetrating to the glass slide, where they would induce emission of undesired X-rays. Ryan & Griffin (1993) discussed, in considerable detail, the advantages and disadvantages of various reported geometric arrangements of beam, sample, optical microscope and detector. In all cases, a reproducible specimen–detector geometry is ensured by placing each successive specimen-surface in the focal plane of the microscope. In most proton microprobes, the beam impacts the specimen at 90°, and the X-ray take-off angle is 45°; this is the case in the CSIRO instrument (Sie *et al.* 1990), which employs an Ealing reflecting objective to provide normal optical viewing of the sample (magnification 150×). In the Guelph instrument (Perujo *et al.* 1988), which was designed around the light optics taken from a defunct ETEK (MAC) electron probe, the beam impact angle is 45°, and the optical axis is normal to the sample with magnification of 300×. The main price of this high optical magnification is an increased background in the spectrum due to the 90° detector placement. Generally, the specimen may be viewed in reflected or transmitted light *via* a

color CCTV camera mounted on the microscope. The stage is driven by computer-controlled stepping motors. The charge incident on each specimen is measured by a current integrator coupled to a scaler, and in order to minimize errors due to secondary-electron emission from the specimen, a suppressor grid biased at negative voltage is placed in front of the specimen. The issue of electronic dead-time is avoided in the Guelph system through the use of an on-demand beam deflector (Teesdale & Campbell 1990). Each time an X ray is detected, this device removes the beam from the final aperture preceding the specimen, and holds it deflected until the signal processing is complete. This approach, common in conventional PIXE but not in micro-PIXE, has the added advantages of minimizing pile-up of pulses, which causes undesired extra peaks in the spectra, and of minimizing specimen heating and damage.

X-ray spectrometer

As PIXE is primarily an analytical technique for trace elements, the geometrical efficiency afforded by energy-dispersion Si(Li) detectors is mandatory, and wavelength-dispersion spectroscopy is precluded. The peaks in the Si(Li) spectra are predominantly Gaussian in shape. The centroid channel of a peak is linearly related to the X-ray energy, and the square of its width is similarly related; the spectrometer is therefore described by four parameters that may vary slightly with time. As an example, Figure 2 shows the spectrum of the USGS basalt glass standard BHVO–1.

The X rays of all elements present above detection limits are recorded simultaneously in the Si(Li) spectrum. An interesting difference from electron probe micro-analysis (EPMA) is the use of absorbing filters to "tailor" the X-ray spectrum. One of the

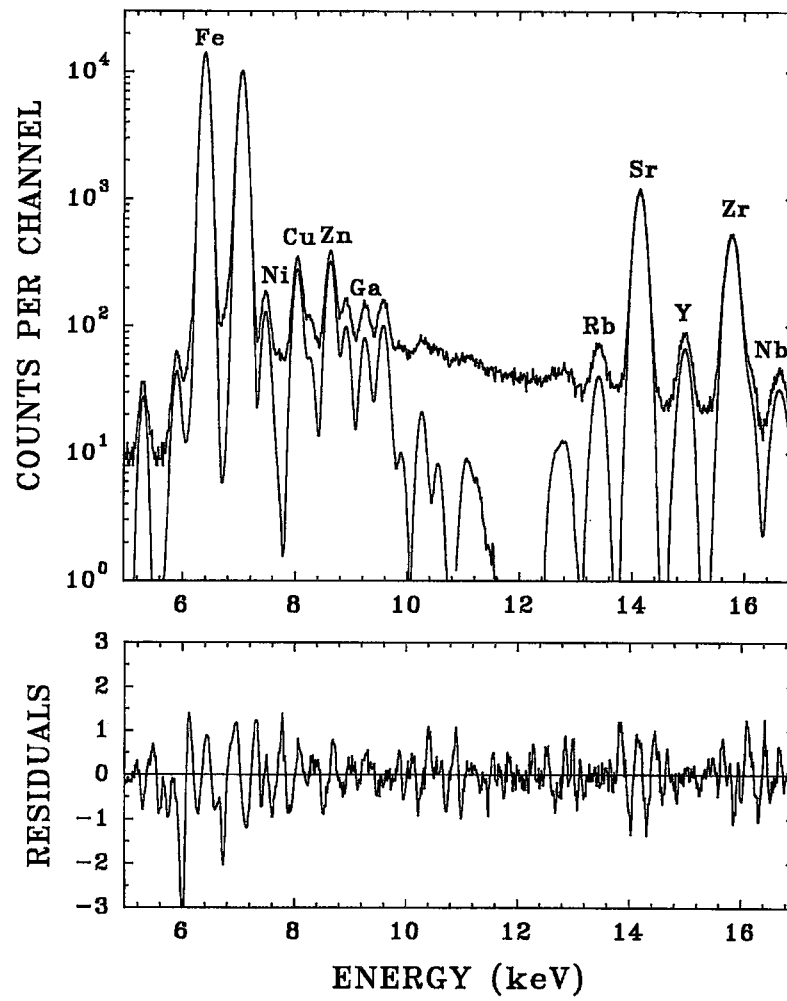

FIG. 2. PIXE spectrum recorded at Guelph from the USGS BHVO–1 basaltic glass standard. The spectrum was recorded using 2.5 μC of 3 MeV protons, and an aluminum filter 250 μm thick. The full curve represents the fitted model-spectrum, which contains characteristic X-rays only; the residuals are in units of one standard deviation.

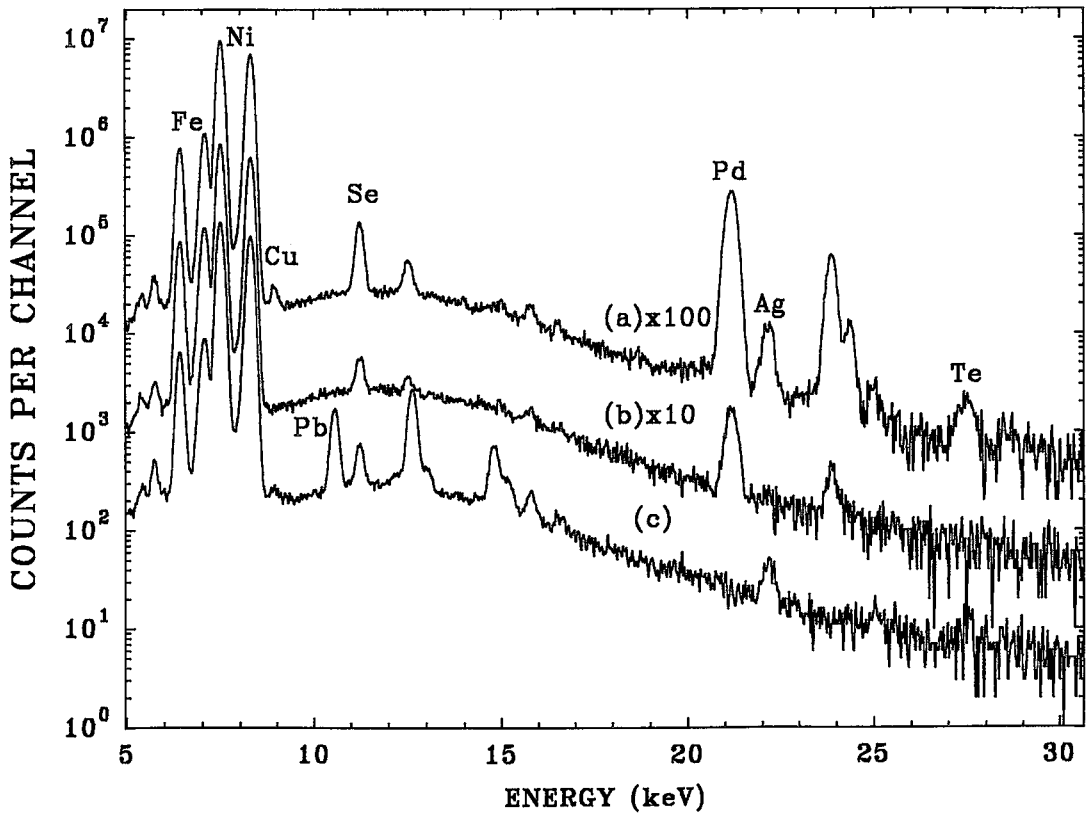

FIG. 3. PIXE spectrum of three samples of Noril'sk pentlandite (Czamanske *et al.* 1992): the spectra were recorded using 10 μC of 3 MeV protons and an aluminum filter 352 μm in thickness. (a) Cu-rich vein ore free of pyrrhotite (Po) from the Medvezhy Creek open pit; (b) Po-bearing ore; (c) Cu-rich Po-free ore, both from the Kharaelakhsky orebody. Concentrations (ppm): (a) Se 261, Pd 2540, Ag 112, Te 54; (b) Se 80, Pd 132; (c) Se 116, Pd <5, Ag 34, Te 36, Pb 1416 (Czamanske *et al.* 1992).

earliest micro-PIXE applications, the analysis of sulfide minerals for silver and platinum-group elements at low concentrations, provides an example. Typical detectors are limited to counting rates of a few thousand counts per second. As the X-ray yield decreases strongly with increasing atomic number, the electronic throughput will be dominated by the X rays of the major elements (S, Fe, Ni, Cu, Zn, *etc.*), whereas the X rays of the trace elements that are of primary interest make negligible contribution. The high count-rates of the major-element X-rays cause pile-up peaks that have a deleterious effect on the detection limits for trace elements. Insertion of an aluminum absorber a few hundred micrometers in thickness reduces the matrix X-ray intensity by a factor of around 1000 (and eliminates the X rays due to sulfur) while transmitting most of the X rays of the trace elements. With the beam current increased to restore the previous count-rate, these X rays now constitute a much increased fraction of the intensity of the spectrum overall, and a detection limit of a few ppm is attained. To illustrate results obtained with a 250-μm Al filter, Figure 3 shows spectra from three samples of pentlandite from Noril'sk containing different concentrations of Pd and other trace elements (Czamanske *et al.* 1992). The use of a wide variety of filters to optimize the analysis of a range of minerals is described by Ryan *et al.* (1990).

A knowledge of the Si(Li) detector's intrinsic efficiency as a function of X-ray energy is necessary. For the typical 5-mm-thick device, this is essentially unity at X-ray energies between 5 and 20 keV. At higher X-ray energies, it falls off slowly, reflecting the absorption in the finite thickness of silicon. At lower X-ray energies, it falls away steeply owing to X-ray attenuation in the beryllium entry-window, a possible surface-layer of ice, the metallic front-contact and the surface silicon dead-layer. All of the detector properties necessary for an accurate knowledge of the efficiency may

be measured (Maenhaut & Raemdonck 1984), and primary and secondary radionuclide standards can provide the absolute efficiency directly (Campbell & McGhee 1986, Denecke *et al.* 1990).

Beam sweeping

Both electric and magnetic means may be used to raster the beam over the specimen surface for the purpose of producing elemental distribution maps. With wide-bore focusing quadrupoles, the deflection system may be placed before the focusing system, and this arrangement provides a large scan-area; for example, the widely used Oxford Microbeams system uses a ferrite-cored magnetic box deflector, which scans 3 MeV protons over an area 2.5 × 2.5 mm (Grime *et al.* 1991). With narrow-bore quadrupole lenses, such an arrangement can drive the beam into the periphery of the bore, where the field diverges from pure quadrupole, resulting in aberrations. It is then better to locate the deflection system after the focusing lenses; the disadvantage is that owing to the shorter distances involved, the imaged area is smaller. In the Guelph microprobe, two pairs of electrostatic deflector plates are located at the entry to the specimen chamber; they derive their potentials from a programmable high-voltage power supply, scanning the beam over a 0.6 × 0.6 mm area. In addition to 2-*D* imaging, most scanning proton microprobes also offer 1-*D* imaging by sweeping the beam back and forth along a line upon the specimen surface; this is particularly useful in studies of chemical zoning.

Microprobe Control and Data Acquisition

The control system must position both the specimen and the beam, whereas the data system must acquire spectral data from analog-to-digital converters and from scalers (*e.g.*, integrated charge, time, *etc.*). Real-time display of energy spectra and of both 1-*D* and 2-*D* images is necessary, and rapid processing of spectra and images to provide data on concentration is highly desirable. Lövestam (1993) has reviewed the three general approaches that have been taken to integrate these functions. The simplest approach employs a single, small microcomputer, and this is exemplified by the 486-type computer employed at Guelph. At the next level of sophistication, the time-consuming input/output functions are handled by a front-end control–acquisition system (*e.g.*, VME bus) while a host computer (*e.g.*, VAX station) controls the sorting of data and the production of element-distribution maps. More advanced solutions utilize several computers and processors.

The two microprobes that were developed specifically for geological work (Sie *et al.* 1990, Perujo *et al.* 1988) are fully automated. In the spot-analysis mode, the spots are first selected by the operator using the microscope and CCTV camera, and then they are analyzed sequentially under microcomputer control, each being exposed to the proton beam for a preset amount of integrated beam-charge. A large number of spectra may be processed in batch mode upon conclusion of the measurements, or the spectra can be processed as they are generated. Even in the most complex cases, concentrations can be obtained and printed for a given spectrum in a few minutes; this permits the operator to adjust the analytical protocol on the basis of the data flow.

Several different approaches have been taken for the creation of element-distribution maps. Each event that contributes to such a map comprises the x and y position signals from the beam-scanning device, together with the corresponding digitized X-ray energy signal (E). The map dimensions are typically 128 × 128 or 256 × 256 pixels. In the simplest method, the maps are generated on-line (Grime *et al.* 1991). An energy window is defined in the X-ray spectrum to include the principal peak of each element of interest; each such window corresponds to an elemental map. Detection of an event within a given window then results in the augmentation by one count of the appropriate pixel in the corresponding map. Although convenient and fast, this approach does not preserve all details of the original spectral data, and it does not permit later reprocessing with different window-definitions. Another method involves collecting all (x, y, E) events in list mode on disk (O'Brien & Legge 1988). With a given set of windows, distribution maps may be displayed on-line during the measurement (Teesdale *et al.* 1993); when the measurement is concluded, all the data taken are available for reprocessing, and there is the further advantage that the time sequence of stored events may be of help in assessing if specimen damage has occurred. Although the storage of all events is more expensive in terms of memory than the storage of one set of distribution maps, recent technical advances are such that this is no longer such a serious drawback.

Data Reduction

In the spectra accumulated in spot-analysis mode, the intensities of the different X-ray lines provide corresponding elemental concentrations. The issues of spectrum processing to obtain these intensities and of the subsequent conversion of intensities to concentrations (involving standards, matrix effects, *etc.*) are intertwined. However, in the interests of convenience, we now review the spectrum-processing aspect, leaving some matters to be clarified in the later discussion of quantitative analysis.

Micro-PIXE spectra generally contain more information than those encountered in EPMA, as they contain X-ray lines not just from major and minor elements, but also from trace elements. Because peak-

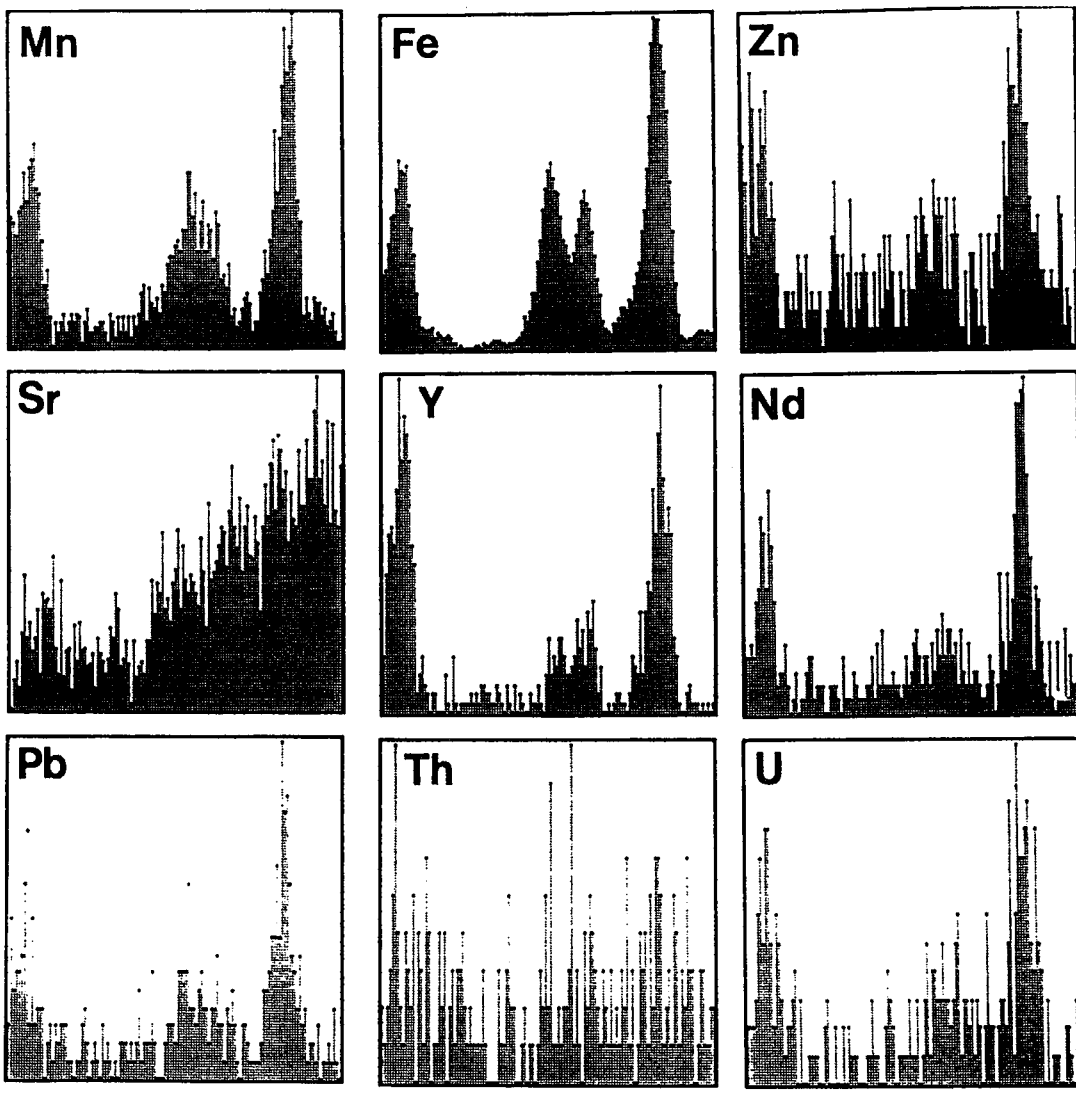

FIG. 4. Example of a linescan across several cracks in a quartz crystal next to metamict britholite (Halden *et al.* 1995b).

to-background ratios can be very large, the Gaussian lineshape of the Si(Li) detector should be modified to describe the non-negligible low-energy tails caused by detector imperfections (Campbell 1990). The usual approach involves least-squares fitting a model PIXE spectrum to the measured one (Ryan *et al.* 1990, Maxwell *et al.* 1989). The model includes a quasi-Gaussian line for every X ray, and both double and triple pile-up. It uses a database comprising the (generally) well-known relative X-ray energies and line intensities in the *K* and *L* series in the X-ray energy region between 1 and 40 keV. For each element surmised to be present, the height (or area) of the dominant X-ray line is a variable of the fit; the other line-intensities for the element are normalized to the principal line *via* the database. The database intensities are modified by transmission through any absorbers, by the detector's intrinsic efficiency and by matrix effects within the specimen. A knowledge of the matrix effects demands knowledge of major-element concentrations (*e.g.*, by a prior EPMA analysis); the issue of matrix effects is dealt with in the next major section.

So that small changes in the detector calibration may be handled easily, it is customary to include the four detector-calibration parameters in the set of fitted variables. The fitting procedure is therefore nonlinear.

Various means have been used to deal with the continuous background. Some approaches model this by rather complex semi-empirical functions, some of whose coefficients are variables of the fit. Others use peak-stripping methods to reduce the spectrum to background, and then augment the peak model by this background in the least-squares fit. We have adopted the top-hat filter approach common in EPMA; a convolution filter function designed to remove spectrum components that are approximately linear in their energy-dependence is applied to both the measured spectrum and the peak-model spectrum, and the fitting procedure is done using these filtered spectra (Maxwell *et al.* 1989). Ryan *et al.* (1988) have developed a sophisticated iterative peak-stripping method that minimizes the undesired influence of major lines upon definition of the background contiguous to them, and they have demonstrated the high accuracy that this provides in dealing with very small peaks located close to the strong peaks of major elements.

In the imaging mode, "windows" are defined in the X-ray spectrum to encompass the peaks of interest; during the construction of the element-distribution maps, all events in each window are assigned to the element concerned. Continuous background-counts will be present in each window, as will overlapping X rays of other elements; distribution maps prepared in this way are therefore semiquantitative and do not directly reflect concentrations. The most effective presentation of distribution maps is in false color, which has been extensively used in the proton-microprobe field. Once a 2-*D* image has been constructed, regions of interest for subsequent spot or 1-*D* analysis generally become apparent. Such subsequent analysis of spots is important in providing quantitative data on concentrations to supplement the semiquantitative information conveyed by the image. One-dimensional line scans provide improved precision relative to 2-*D* images, and the need for color disappears. We give one example in Figure 4; in this case, the proton beam has scanned over several cracks in a sample of quartz, and the presence of elements that were probably deposited by fluid in these cracks is shown. In a recent development, Ryan & Jamieson (1993) have introduced a dynamic on-line method for making background and overlap corrections during 1-*D* and 2-*D* image construction. The resulting distribution maps thus reflect concentration directly. This new approach is effective even when the matrix composition varies significantly across the region that is being imaged.

Quantitative Analysis

General principles

The proton–specimen interaction involves the slowing down of the proton, with consequently decreasing cross-section for X-ray production along its linear path, the ionization of a particular atom, and the transmission of the resulting X-ray through the specimen to the detector. The physics is straightforward (Johansson & Campbell 1988) and leads to an expression of the form

$$I(Z) = C_Z Q H \varepsilon_Z t_Z I_1(Z,M) \quad (1)$$

for the intensity of X rays of element Z whose concentration is C_Z. Q is the proton charge (usually in μC), H an instrumental constant that subsumes detector solid-angle and any calibration factor in the charge integrator; ε_Z is the intrinsic efficiency of the X-ray detector; t_Z is the transmission of the X ray of interest through any absorber foils being used; $I_1(Z)$ is the computed theoretical X-ray intensity per unit proton charge per steradian and per unit concentration, and is in practice obtained by numerical integration along the linear track of the proton. $I_1(Z)$ is analogous to $\phi(\rho z)$ in EPMA, but unlike that quantity, it can be calculated directly and accurately because of the simple physics and accurate database. It describes the matrix effects, *i.e.*, the role of the major and minor elements in slowing down the protons and attenuating the X rays generated, and therefore by definition includes the concentrations of all elements present. There are also contributions to the X-ray intensities arising from the secondary process of fluorescence of constituents by the intense X-rays of the major elements. This process can be modeled accurately, and is included in current PIXE software. The overall database is therefore an extensive one, containing proton-ionization cross-sections and stopping powers, X-ray-attenuation coefficients and photoelectric cross-sections.

Trace-element analysis in a known matrix

The simplest application of micro-PIXE is trace-element analysis of a specimen whose major-element concentrations are known. In such a case, the matrix integrals $I_1(Z,M)$ can be computed directly for the X rays of each trace element Z, and the measured X-ray intensities of the trace elements $I(Z)$ converted directly to concentrations *via* eq. (1). This tandem approach has been widely used. Remond *et al.* (1987) showed the complementary use of EPMA and micro-PIXE for various trace elements in a wide range of sphalerite samples. They found good agreement between the two methods.

For trace elements of atomic number Z greater than 20, the database is very accurate, and the quantity $I_1(Z,M)$ can be calculated with accuracy commonly better than 5%. The detector efficiency can be obtained with an accuracy of 1–2%. Thus in principle, trace-element analysis by micro-PIXE has potentially excellent accuracy (see below for examples). The instrumental constant H may be determined with various types of standard. We have used NIST alloy standards (*e.g.*, SRM 1155) that contain several minor

elements spanning the entire region of atomic number of interest to us; they provide a useful check on the expected constancy of H across the elements of interest. Inhomogeneity on a micrometer scale in such standards demands that the microbeam be rastered over an area some hundreds of square micrometers. We have also used the CANMET suite of synthetic pyrrhotite compositions containing 0.1% each of Pd (homogeneously distributed) and Se (not so). There is clearly merit in adopting geochemical standards whose matrix is similar to the specimens of interest; thus we have recently used Sr and Fe in the USGS BHVO–1 basaltic glass standard for the analysis of silicates. Others (*e.g.*, Ryan *et al.* 1990) have standardized relative to a known major element within the specimen of interest, which provides the optimum situation with regard to similarity of matrix.

Major elements

PIXE is also capable of determining the concentration of major elements comprising the matrix, although the solution of the set of eq. (1) now has to be an iterative one, as these unknown concentrations are required to evaluate the quantities $I_1(Z,M)$. In precise analogy to EPMA, a starting set of major-element concentrations is estimated, the matrix integrals are computed, the spectrum is fitted to provide X-ray intensities, and the intensity *versus* concentration equations are solved to give a new set of concentrations. This cycle is repeated until a consistent set of concentrations emerges. Because the elements Na, Mg, Al and Si are commonly of interest, no X-ray absorbers can be used, and to avoid back-scattered protons entering the X-ray detector, the beam energy is much reduced (to 0.75 MeV in our case). In oxide minerals, the X rays emitted by oxygen do not penetrate the detector window, and oxygen is dealt with by associating the stoichiometric quantity of oxygen with each cation.

The accuracy of the database worsens for atomic numbers below 20, and in this region, the steeply changing efficiency of the detector (owing in part to a time-dependent surface layer of ice) is a potential source of error. We find it preferable to have a single-element standard for each element that is present, and to augment these where necessary with simple compounds or silicate minerals (Campbell & Teesdale 1993). The equations to be solved are of the form

$$\frac{C_Z(SP)}{C_Z(ST)} = \frac{I_Z(SP)}{I_Z(ST)} \cdot \frac{Q(ST)}{Q(SP)} \cdot \frac{I_1(Z,ST)}{I_1(Z,SP)} \qquad (2)$$

where SP, ST denote specimen and standard. Two examples of recent major-element determinations in our laboratory are shown in Table 2. The materials analyzed are on a polished mineral multi-mount, type MINM25–53, supplied by Astimex Ltd. of Toronto.

TABLE 2. REPRESENTATIVE COMPOSITION OF SANIDINE AND PENTLANDITE OBTAINED BY PIXE

Sanidine	O	Na	Aℓ	Si	K	Fe	Ba
R	46.28	2.23	9.93	30.23	10.05	0.14	0.98
M	47.1	2.2	9.7	29.7	10.3	0.13	1.0
E		0.15	0.12	0.2	0.2	0.04	0.2

Pentlandite	S	Fe	Co	Ni
R	33.01	30.77	0.10	36.12
M	31.9	30.8	<0.45	36.0
E	0.2	1.1		1.6

R = recommended value of concentration (wt %)
M = measured concentration (wt %)
E = 1σ error estimate (counting statistics and fitting error only)

The pentlandite case is chosen to complement the trace-element data on pentlandite in Figure 3.

Inclusions

Ryan *et al.* (1990) and Campbell *et al.* (1993) have developed formalisms to model X-ray production in subsurface layers. Ryan *et al.* (1993) have extended this from simple layers to a variety of realistic shapes for subsurface inclusions, allowing analysis of fluid inclusions in a nondestructive manner.

Accuracy, precision and detection limits

The various physical factors that bear upon accuracy include smoothness of the specimen surface, geometrical alignment of beam, specimen and detector, charge integration and suppression of secondary electrons, and efficiency of the X-ray detector. The database is clearly crucial, and there is a continuing need to improve it, especially for *L* and *M* X-rays. The software used for spectrum-fitting and standardization also is critical, especially in situations where weak peaks have to be distinguished from intense overlapping neighbors. Precision or reproducibility of concentration data is influenced by counting statistics, by the reproducibility of the above physical factors, and by the homogeneity of the specimen on the micrometer scale. The literature contains many demonstrations of accuracy, from which we select a few examples. Much of the early PIXE work on sulfide minerals involved EPMA analysis, and good agreement between the two methods was obtained.

Ryan *et al.* (1990) fused three USGS rock-powder standards, BCR–1, AGV–1 and GSP–1, to form glasses, and analyzed these using a beam spot about 20 μm in diameter. The average concentrations from eight different spots on each specimen were found to be in good agreement with accepted values, demonstrating the accuracy of micro-PIXE at levels of concentration down to 10 ppm. However, the ratio h of observed standard deviation to the statistical uncertainty was respectively 1.8, 2.4 and 5.6, indicating considerable

TABLE 3. COMPOSITIONAL DATA ON SILICATE GLASS STANDARDS AS OBTAINED BY MICRO-PIXE ANALYSIS

	BHVO-1				DR-1-P3-4			
	C_o	C	ϵ	LOD	C_o	C	ϵ	LOD
Mn[a]	1300	1316	27	40	—	1280	27	40
Fe	8.64%	8.67%	7	—	—	8.91%	—	—
Ni[a]	121	128	9	11	58	27	30	13
Cu[b]	136	162	4	6	44	39	4	6
Zn[b]	105	116	3	5	134	130	3	5
Ga[b]	21	23	2	3	—	—	—	3
Rb[c]	11	9.4	1	3	44.2	46	2	3
Sr[c]	403	401	3	3	—	912	5	3
Y[c]	27.6	25.5	1.5	2	38.3	35	2	4
Zr[c]	179	172	5	11	338	359	7	18
Nb[c]	19	18	1.5	3	50.7	57.5	2	3
Ba[c]	139	114	27	50	418	465	40	56

C_o = nominal concentration (ppm)
C = measured concentration (ppm)
ϵ = uncertainty (1 standard deviation in ppm) of a single measurement
LOD = limit of detection (ppm) in a single 3-minute measurement

a) Mean of 10 measurements using a 106 μm Al filter;
b) Mean of 10 measurements using a 247 μm Al filter;
c) Mean of 20 measurements using a 247 μm Al filter.

From Czamanske *et al.* (1993) with permission of the Mineralogical Society of America.

inhomogeneity. The authors therefore expressed their preference for a standardless method in which they normalize to the known concentration of a particular major element (Fe in the examples cited). Table 3 reproduces results from a similar exercise (Czamanske *et al.* 1993) using the standard BHVO–1 fused to a highly homogeneous glass, and the natural Tahitian Seamount basaltic glass DR–1–P3–4. Czamanske *et al.* examined an extensive suite of well-characterized silicate glasses and minerals, including Kakanui augite and hornblende, and natural samples of volcanic glass, amphibole, pyroxene and garnet; they found excellent agreement between micro-PIXE results and accepted concentrations.

Figure 5 shows the results of a remarkable PIXE analysis by Woolum *et al.* (1987). Two specimens of carbonaceous chondrite were studied in a measurement lasting several hours, the object being to compare concentrations with compiled best values over a very wide range of concentrations. The figure shows a remarkable degree of agreement. Of course, the very low limits of detection achieved in such lengthy measurements will not be attained in routine micro-PIXE analysis of large suites of specimens. However, this work does serve well to show the ultimate in accuracy and detection limits.

Minimum detection-limits (MDLs) are defined as the concentrations that would result in a peak intensity that is just discernible above background. Interference-free limits represent the ultimate that can be attained, and assume the absence of elements that would contribute overlapping peaks. It is more generally the case to work with practical detection-limits that take into account not only the continuum but also the influence of whatever overlaps are typical for a given suite. The statistical criterion is that the peak intensity contained within one full-width at half-maximum be equal to three standard deviations of the background intensity in that region. MDLs are in no way absolute. They can be decreased by amassing more counts in the spectrum, and thus they decrease in inverse proportion to the square root of increased measurement time or beam current. However, economics limits the former, and specimen damage limits the latter. As a larger beam-spot is less damaging, the spot size also plays an important role.

The major elements in a specimen influence trace-element MDLs in various ways. One obvious way is through line overlap; in an iron-rich specimen, the MDL for Co, whose $K\alpha$ line overlaps the Fe $K\beta$ line, is significantly higher than those of Ni, Cu, Zn, *etc.* Another is line proximity. In zircon, for example, the pronounced tailing feature (due in large part to Compton scattering in the specimen) left of the intense Zr *K* peak worsens the MDL for Y, whose *K* X-ray line is superimposed on that artefact. When the major elements are of low atomic number, their X rays can dominate the spectrum to such an extent that the X rays generated by the trace elements contribute only negligibly to the overall count-rate; this necessitates the use of absorbing filters to suppress major-element lines in favor of the more energetic trace-element lines.

Figures 6 and 7 indicate some of our recent experience in spot analysis using optimized X-ray absorbers; they are chosen to correspond to specimens that generate spectra of the type shown in Figures 2 and 3. For elements detected *via* their *K* X-rays, the optimum MDLs occur in the region of $Z = 25$. At lower *Z*, yields of *K*-shell fluorescence fall off, as does detector efficiency. At higher *Z*, the proton ionization cross-sections fall steeply. The same behavior is noted for heavier elements detected *via* their *L* X-rays. We present elsewhere (Campbell *et al.* 1993) a more extensive set of MDL examples, encompassing matrices of quartz, garnet, pentlandite, calcite, apatite and titanite.

The MDLs attained in 1-*D* and 2-*D* imaging are increasingly larger than those for point analysis, reflecting the fact that an image comprises many such points. However, one is usually prepared to compensate to some degree by devoting longer times to imaging than to spot analysis. It is then possible to image the distribution of trace elements, as will be demonstrated by examples in the next paper (Halden *et al.* 1995a). In studies of chemical zoning, grain boundaries and surfaces, micro-PIXE provides a valuable extension to EPMA. The latter can provide images of the distributions of major and minor elements. Micro-PIXE then provides the corresponding trace-element distributions, which may either be coupled to or decoupled from the major-element variations.

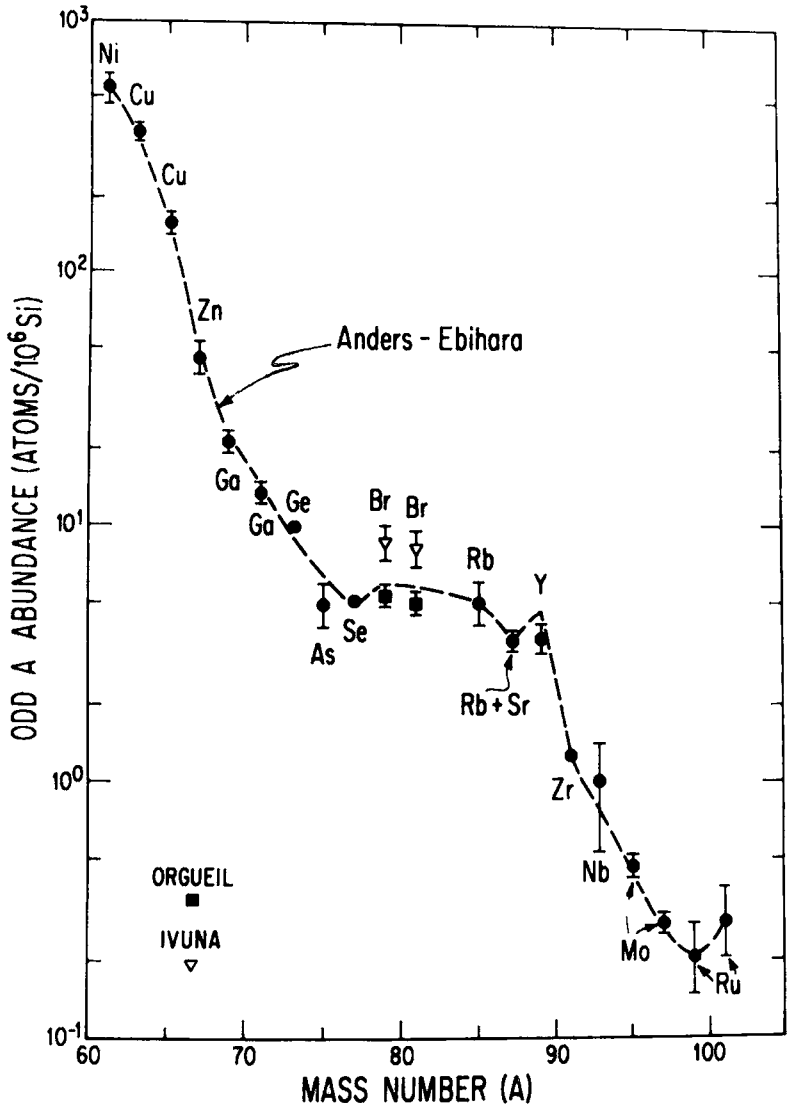

FIG. 5. Atomic abundances in two samples of carbonaceous chondrite as measured by PIXE (Woolum *et al.* 1987). The data were recorded using 1 mC of 3 MeV protons; an Al filter 140 μm in thickness was employed. The data are normalized to nickel using the Ni abundance of Anders & Ebihara (1982). The abundances of the Anders–Ebihara compilation are shown as the dashed curve.

AUXILIARY TECHNIQUES

An attractive feature of the proton microprobe is that a number of additional techniques may be brought to bear in spot analysis or imaging mode. Nuclear reaction analysis (NRA) has been developed alongside PIXE, and tends to be useful for specific elements where convenient reactions exist. Protons induce useful amounts of gamma-ray emission from a small number of very light elements, and this has been used for analysis of samples for sodium and fluorine (Johansson & Campbell 1988). However, if full advantage is to be taken of NRA, additional beams such as helium and deuterium are required. For example, Heymann *et al.* (1988) used a deuterium beam to study glass inclusions in chondrites, combining PIXE analysis for the trace elements with simultaneous NRA analysis of the distribution of carbon. A more detailed summary of work

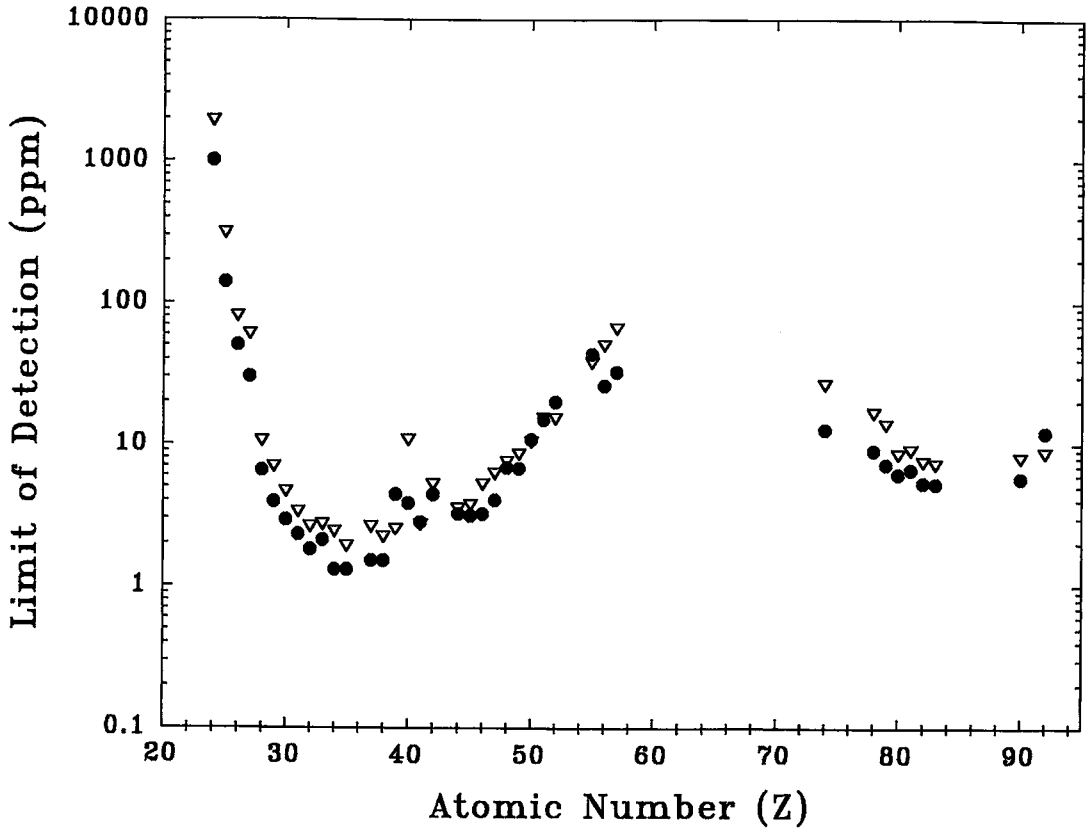

FIG. 6. Limits of detection for trace-element analysis of silicate minerals. Triangles represent the BHVO–1 basaltic glass, and filled circles, a rhyolite glass. Energy of proton beam: 3 MeV; collected charge: 2.5 μC; beam spot: 5 × 10 μm: filter 250 μm Al (figures based on data from Czamanske *et al.* 1993).

using NRA methods is given by Ryan & Griffin (1993). The analogue of cathodoluminescence, ionoluminescence, has recently been used; it is observed *via* the incorporation of an optical spectrometer in the micro-PIXE facility in Lund, Sweden (Yang *et al.* 1993); in that work, which concerns zircon, the ionoluminescence reveals zoning, suggesting that ionoluminescence may be a useful adjunct to micro-PIXE.

CONCLUDING REMARKS

Much of the development work needed to establish micro-PIXE as a quantitative technique is now complete. However, the expertise required for routine, accurate micro-analysis of geological specimens is confined to a small number of laboratories. Micro-PIXE, especially when complemented by other ion-beam techniques, extends the range of analytical tools available to geologists, and its use can be expected to grow rapidly.

ACKNOWLEDGEMENTS

This work was supported by the Natural Sciences and Engineering Research Council of Canada through operating grants to NMH and JLC and through equipment grants to JLC. We are most grateful to the reviewers, Associate Editor F.C. Hawthorne and R.F. Martin for their thorough critiques of the original manuscript.

REFERENCES

ANDERS, E. & EBIHARA, M. (1982): Solar system abundances of the elements. *Geochim. Cosmochim. Acta* **46**, 2363-2380.

CAMPBELL, J.L. (1990): X-ray spectrometers for PIXE. *Nucl. Instrum. Methods Phys. Res.* **B49**, 115-125.

_____, HIGUCHI, D., MAXWELL, J.A. & TEESDALE, W.J. (1993): Quantitative PIXE microanalysis of thick specimens. *Nucl. Instrum. Methods Phys. Res.* **B77**, 95-109.

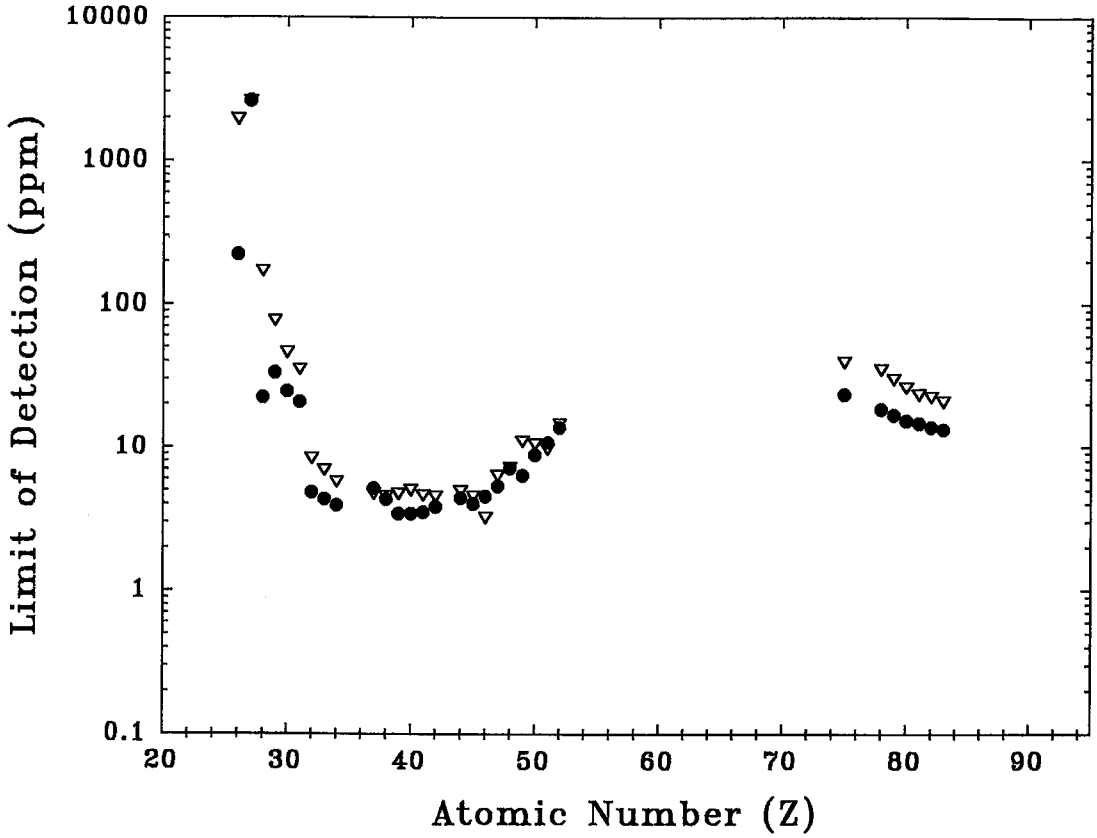

FIG. 7. Limits of detection for trace-element analysis of sulfide minerals. Triangles represent pentlandite (350 μm Al filter), filled circles, pyrrhotite (250 μm Al filter). Energy of proton beam: 3 MeV; collected charge: 10 μC; beam spot: 5 × 10 μm (figures based on data from Czamanske *et al.* 1992).

———, MAXWELL, J.A., TEESDALE, W.J., WANG, J.-X. & CABRI, L.J. (1990): Micro-PIXE as a complement to electron probe microanalysis in mineralogy. *Nucl. Instrum. Methods Phys. Res.* **B44**, 347-356.

——— & MCGHEE, P.L. (1986): State-of-the-art efficiency determination for a Si(Li) X-ray detector in the 3–40 keV energy range. *Nucl. Instrum. Methods Phys. Res.* **A248**, 393-404.

——— & TEESDALE, W.J. (1993): Micro-PIXE analysis of major elements in mineral specimens. *Nucl. Instrum. Methods Phys. Res.* **B74**, 503-510.

CZAMANSKE, G.K., KUNILOV, V.E., ZIENTEK, M.L., CABRI, L.L., LIKHACHEV, A.P., CALK, L.C. & OSCARSON, R.L. (1992): A proton microprobe study of magmatic sulfide ores from the Noril'sk–Talnakh district, Siberia. *Can. Mineral.* **30**, 249-287.

———, SISSONS, T.W., CAMPBELL, J.L. & TEESDALE, W.J. (1993): Micro-PIXE analysis of silicate reference standards. *Am. Mineral.* **78**, 893-903.

DENECKE, B., BAMBYNEK, W., GROSSE, G., WÄTJEN, U. & BALLAUX, C. (1990): A set of X-ray fluorescence reference sources for the intrinsic efficiency calibration of Si(Li) detectors down to 1 keV. *Nucl. Instrum. Methods Phys. Res.* **B49**, 152-156.

GRIME, G.W., DAWSON, M., MARSH, M., MCARTHUR, I.C. & WATT, F. (1991): The Oxford submicron nuclear microscopy facility. *Nucl. Instrum. Methods Phys. Res.* **B54**, 52-63.

HALDEN, N.M., CAMPBELL, J.L. & TEESDALE, W.J. (1995a): Micro-PIXE in mineralogy and geochemistry. *Can. Mineral.* **33**, 293-302.

———, ——— & ——— (1995b): Scanning proton microprobe mapping of rare elements in mineral cleavages, fractures and grain boundaries: evidence for rare-element mobility. *Can. Mineral.* **33** (in press).

HEYMANN, D., MAKJANIC, J., VAN DER STAP, C.C.A.H., VIS, R.D. & VERHEUL, H. (1988): Carbon, oxygen, silicon,

sulfur, calcium and iron determination in 24 dark clasts and one dark inclusion of the Allende meteorite by $^{12}C(d,p)^{13}C$ nuclear reaction and PIXE. *Meteoritics* **23**, 131-137.

JOHANSSON, S.A.E. & CAMPBELL, J.L. (1988): *PIXE: a Novel Technique for Elemental Analysis.* John Wiley and Sons, Ltd., Chichester, U.K.

LEGGE, G.F.J., LAIRD, J.S., MASON, L.M., SAINT, A., CHOLEVA, M. & JAMIESON, D.N. (1993): High resolution imaging with high energy ion beams. *Nucl. Instrum. Methods Phys. Res.* **B77**, 153-168.

LÖVESTAM, N.E.G. (1993): Currently used control and data acquisition systems nuclear microprobes. *Nucl. Instrum. Methods Phys. Res.* **B77**, 71-78.

MACARTHUR, J.D. & MA, XIN-PEI (1991): A review of particle-induced X-ray emission in geology. *Int. J. PIXE* **1**, 311-338.

MAENHAUT, W. & RAEMDONCK, H. (1984): Accurate calibration of a Si(Li) detector for PIXE analysis. *Nucl. Instrum. Methods Phys. Res.* **B1**, 123-136.

MARTIN, F.W. & GOLOSKIE, R. (1988): Simultaneous compensation of second order parasitic aberrations in both principal sections of an achromatic quadrupole lens doublet. *Nucl. Instrum. Methods Phys. Res.* **B30**, 242-247.

MAXWELL, J.A., CAMPBELL, J.L. & TEESDALE, W.J. (1989): The Guelph PIXE software package. *Nucl. Instrum. Methods Phys. Res.* **B43**, 218-230.

O'BRIEN, P.M. & LEGGE, G.F.J. (1988): High-speed acquisition and handling of scanning proton microprobe data. *Nucl. Instrum. Methods Phys. Res.* **B30**, 312-316.

PERUJO, A., RIDDOLLS, T.R. & CAMPBELL, J.L. (1988): Design of a dedicated target chamber for PIXE microanalysis of mineral samples. *Nucl. Instrum. Methods Phys. Res.* **B30**, 280-283.

REMOND, G., CESBRON, F., TRAXEL, K., CAMPBELL, J.L. & CABRI, L.J. (1987): Electron microprobe analysis and proton-induced X-ray spectrometry applied to trace element analysis in sulfides: problems and prospects. *Scanning Microscopy* **1**, 1017-1037.

RYAN, C.G., CLAYTON, E., GRIFFIN, W.L., SIE, S.H. & COUSENS, D.R. (1988): SNIP, a statistics-sensitive background treatment for the quantitative analysis of PIXE spectra in geoscience applications. *Nucl. Instrum. Methods Phys. Res.* **B34**, 396-402.

_____, COUSENS, D.R., SIE, S.H., GRIFFIN, W.L., SUTER, G.F. & CLAYTON, E. (1990): Quantitative PIXE microanalysis of geological material using the CSIRO proton microprobe. *Nucl. Instrum. Methods Phys. Res.* **B47**, 55-71.

_____ & GRIFFIN, W.L. (1993): The nuclear microprobe as a tool in geology and mineral exploration. *Nucl. Instrum. Methods Phys. Res.* **B77**, 381-398.

_____, HEINRICH, C.A. & MERNAGH, T.P. (1993): PIXE microanalysis of fluid inclusions and its application to study ore metal segregation between magmatic brine and vapour. *Nucl. Instrum. Methods Phys. Res.* **B77**, 463-471.

_____ & JAMIESON, D.N. (1993): Dynamic analysis: on-line quantitative PIXE microanalysis and its use in overlap-resolved elemental mapping. *Nucl. Instrum. Methods Phys. Res.* **B77**, 203-214.

SIE, S.H., RYAN, C.G., COUSENS, D.R. & SUTER, G.F. (1990): A tandetron-based microbeam system. *Nucl. Instrum. Methods Phys. Res.* **B45**, 543-547.

_____, _____ & SUTER, G.F. (1991): Micro-PIXE applications in minerals research. *Scanning Microscopy* **5**, 977-987.

TEESDALE, W.J. & CAMPBELL, J.L. (1990): An on-demand beam deflection system for microbeam PIXE analysis. *Nucl. Instrum. Methods Phys. Res.* **B52**, 93-97.

_____, _____ & HALDEN, N.M. (1993): Two-dimensional mapping of element variation in minerals using the Guelph proton microprobe. *Nucl. Instrum. Methods Phys. Res.* **B77**, 405-409.

WATT, F. & GRIME, G.W. (1987): *Principles and Applications of High Energy Microbeams.* Adam Hilger, London, U.K.

WOOLUM, D.S., BURNETT, D.S., BENJAMIN, T.M., ROGERS, P.S.Z., DUFFY, C.J. & MAGGIORE, C.J. (1987): Trace element contents of primitive meteorites: a test of solar system abundance smoothness. *Nucl. Instrum. Methods Phys. Res.* **B22**, 376-379.

YANG, CHANGYI, LARSSON, N.P.-O., SWIETLICKI, E., MALMQVIST, K.G., JAMIESON, D.N. & RYAN, C.G. (1993): Imaging with ionoluminescence (IL) in a nuclear microprobe. *Nucl. Instrum. Methods Phys. Res.* **B77**, 188-194.

Received June 10, 1993, revised manuscript accepted January 30, 1994.